PNAS RESEARCH ARTICLE | IMMUNOLOGY AND INFLAMMATION

MR1 presents vitamin B6–related compounds for recognition by MR1-reactive T cells

Mitchell P. McInerney[a,1], Wael Awad[a,1], Michael N. T. Souter[b,1], Yang Kang[b,1], Carl J. H. Wang[a], Kean Chan Yew Poa[a], Mohamed R. Abdelaal[a], Ngoc H. Le[a], Chloe M. Shepherd[a], Conor McNeice[a], Lucy J. Meehan[b], Adam G. Nelson[b], Jeremy M. Raynes[a], Jeffrey Y. W. Mak[c], James McCluskey[b], Zhenjun Chen[b], Ching-Seng Ang[d], David P. Fairlie[c], Jérôme Le Nours[a], Patricia T. Illing[a,2], Jamie Rossjohn[a,e,2], and Anthony W. Purcell[a,2]

Affiliations are included on p. 11.

Edited by Gennaro De Libero, University of Basel, Basel, Switzerland; received July 23, 2024; accepted October 12, 2024 by Editorial Board Member Tak W. Mak

The major histocompatibility complex class I related protein (MR1) presents microbially derived vitamin B2 precursors to mucosal-associated invariant T (MAIT) cells. MR1 can also present other metabolites to activate MR1-restricted T cells expressing more diverse T cell receptors (TCRs), some with anti-tumor reactivity. However, knowledge of the range of the antigen(s) that can activate diverse MR1-reactive T cells remains incomplete. Here, we identify pyridoxal (vitamin B6) as a naturally presented MR1 ligand using unbiased mass spectrometry analyses of MR1-bound metabolites. Pyridoxal, and the related compound, pyridoxal 5-phosphate bound to MR1 and enabled cell surface upregulation of wild type MR1*01 and MR1 expressing the Arg9His polymorphism associated with the MR1*04 allotype in a manner dependent on Lys43-mediated Schiff-base formation. Crystal structures of MR1*01 in complex with pyridoxal and pyridoxal 5-phosphate showed how these ligands were accommodated within the A-pocket of MR1. T cell lines transduced with the 7.G5 TCR, which has reported "pan-cancer" specificity, were specifically activated by pyridoxal presented by antigen-presenting cells expressing MR1*01 and MR1 allotypes bearing the less common Arg9His polymorphism. 7.G5 T cells also recognized, to a lesser extent, pyridoxal 5-phosphate and, importantly, recognition of both vitamers was blocked by an anti-MR1 antibody. 7.G5 TCR reactivity toward pyridoxal was enhanced when presented by the Arg9His polymorphism-bearing MR1 allotypes. Vitamin B6, and vitamers thereof, have been associated with various cancers, and here we describe a link between this ligand, MR1, and its allomorphs, and the pan-cancer 7.G5 TCR. This work identifies an MR1 ligand that can activate a diverse MR1-restricted TCR.

MHC class I-related molecule (MR1) | T cell receptor | metabolite | mass spectrometry | structural biology

Significance

This study describes a naturally presented MR1-restricted ligand derived from vitamin B6. The molecular basis of the binding of pyridoxal and pyridoxal 5-phosphate described here reflects the ability of the MR1 A-pocket to accommodate different vitamin scaffolds. This ligand binds covalently to MR1 with moderate affinity and is able to activate reporter cells expressing a "pan cancer" T cell receptor. We postulate that the increased metabolism of vitamin B6 by tumors leads to elevated levels of pyridoxal presentation and preferential recognition of tumors by 7.G5-like T cells.

The antigen-binding clefts of MHC, CD1, and MR1 molecules are ideally suited to bind, respectively, to peptides, lipids, and small-molecule metabolites (1, 2). Structural and mass spectrometry-based studies of MHC–peptide complexes have been extremely informative in understanding the peptide repertoire of given MHC molecules, which has subsequently led to the characterization of neoepitope presentation in tumor immunity for instance, with clinically proven downstream therapeutic applications (3, 4). Furthermore, structural studies have shown how self and foreign lipids can be accommodated by CD1 molecules (5), and recent lipidomics analyses have also provided insight into the repertoire of self-lipids that can bind to the human CD1 isoforms (6). However, the full repertoire of endogenous and foreign small molecule metabolites that can be presented by MR1 still remains unclear.

MR1 is an antigen-presenting molecule that, unlike MHC molecules, exhibits very few polymorphisms. The most prevalent MR1 allomorph is MR1*01, while MR1*02 (His17Arg), and MR1*04 (Arg9His, His17Arg) differ from MR1*01 by one or two residues, respectively, and are encoded by allele groups with frequencies of 71%, 25%, and 1% in the human population (7, 8). Initially, MR1*01 was shown to capture vitamin B2 precursors that are derived from metabolic pathways found in a wide range of microbes, but not in mammals that do not synthesize vitamin B2, and thereby represent a metabolic signature of infection (9, 10). MAIT cells, a highly abundant population of T cells in humans, possess a semi-invariant (TRAV1-2-TRAJ33/20/12) T cell receptor that specifically respond to these MR1-restricted riboflavin-based precursors, of which 5-OP-RU is the most potent MAIT cell antigen described (9, 11, 12). Other classes of MR1 ligands have now been documented, including self-ligands, drug, and drug-like molecules and other microbial

Author contributions: M.N.T.S., J.M., Z.C., P.T.I., J.R., and A.W.P. designed research; M.P.M., W.A., M.N.T.S., Y.K., C.J.H.W., K.C.Y.P., M.R.A., N.H.L., C.M., L.J.M., A.G.N., C.-S.A., and P.T.I. performed research; C.M.S., J.M.R., J.Y.W.M., D.P.F., and J.L.N. contributed new reagents/analytic tools; M.P.M., W.A., M.N.T.S., Y.K., C.-S.A., P.T.I., J.R., and A.W.P. analyzed data; and M.N.T.S., J.M., P.T.I., J.R., and A.W.P. wrote the paper.

Competing interest statement: J.R., D.P.F., and J.M. are inventors on patent applications (PCT/AU2013/000742, WO2014005194; PCT/AU2015/050148, WO2015149130) describing MR1 ligands and MR1-tetramer reagents.

This article is a PNAS Direct Submission. G.D.L. is a guest editor invited by the Editorial Board.

[1]M.P.M., W.A., M.N.T.S., and Y.K. contributed equally to this work.

[2]To whom correspondence may be addressed. Email: patricia.illing@monash.edu, jamie.rossjohn@monash.edu, or anthony.purcell@monash.edu.

This article contains supporting information online at https://www.pnas.org/lookup/suppl/doi:10.1073/pnas.2414792121/-/DCSupplemental.

Published November 26, 2024.

ligands, many of which are either weak MAIT cell agonists or are nonstimulatory and inhibit MAIT cell activity (11, 13–17). In addition to MAIT cells, the advent of MR1 tetramers has enabled the identification of a population of MR1-restricted T cells that do not express the canonical invariant α-chain of the MAIT TCR, but instead exhibit varied αβ TCR gene usage (18–21). These diverse MR1-restricted T cells can be activated in the absence of microbial infection and exhibit distinct ligand specificities compared to MAIT cells (19, 22), including recognition of nucleobase adducts that are formed during cellular stress (14). Moreover, a recent report identified a MR1-restricted TCR, termed 7.G5, that while inert to healthy cells, lysed a large panel of tumor cell lines, and promoted anti-tumor immunity in a MR1- and ligand-dependent manner (23). Some recognition of normal tissues expressing MR1 has also been reported recently (24). Here, using mass spectrometry approaches to probe natural metabolite presentation by cell surface MR1 molecules, we identify pyridoxal as an MR1-restricted antigen, and provide a structural basis of how this ligand is accommodated in the A-pocket of MR1. We subsequently show that while this ligand does not activate a prototypic MAIT TCR A-F7 (25), in the context of MR1*01, the 7.G5 TCR can be activated by this ligand in an MR1-dependent manner that is further enhanced by the Arg9His polymorphism present in the antigen (Ag)-binding cleft of the MR1*04 allotype.

Results

Unbiased Mass Spectrometry Approach to Identify MR1 Ligands. The ligands that bind MR1 have been identified by a series of approaches, including ligand capture by MR1 refolding and mass spectrometry, in silico approaches, as well as structure–activity relationships in MR1 upregulation and MAIT cell activation assays – all of which involve targeted analyses of candidate ligands (for review see ref. 26). We have developed an unbiased ligand identification approach using MR1 purified from cells followed by mass spectrometry to identify the extracted ligands. Our strategy incorporates a series of controlled experiments to distinguish naturally presented MR1 ligands from the abundant chemical background (illustrated by Fig. 1*A*). Namely, we examined differential ligand composition following immunoprecipitation of MR1 molecules from a series of C1R cell transfectants; i) cells overexpressing a mutant MR1 molecule (Lys43Ala) which is unable to form a Schiff base bond with the ligand [C1R.MR1^{K43A} (27)], ii) C1R overexpressing MR1*01 as an abundant source of MR1*01 bound ligands (C1R.MR1*01), and iii) C1R.MR1*01 cells incubated with a high affinity ligand (Ac-6-FP) (28) that should displace endogenous ligands and specifically reduce the signal of ligands isolated from these particular cells. Furthermore, elution from an MHC class I immunoprecipitation and protein G precolumn clean-up were collected and analyzed, to establish and eliminate from consideration, the chemical background signals associated with the immunoprecipitation process.

MR1 complexes were purified from cell lines using immunoaffinity purification, and their bound metabolite cargo was analyzed using a multipronged liquid chromatography–mass spectrometry (LC–MS) approach. We identified a species at m/z 168.07 that was found predominantly in the analysis of MR1*01 molecules purified from the C1R.MR1*01 sample and subsequently identified as the compound pyridoxal (PL) through spectral library matching within MS-DIAL (29), AI-based interrogation of MS/MS data (30), and matching to a retrospectively analyzed PL standard (Fig. 1 *B*–*E*). PL is one of six structurally related compounds (i.e., vitamers) that comprise vitamin B6 (e.g., Fig. 2*A*). The related phosphorylated vitamer pyridoxal 5′-phosphate (PLP) was not identified by LC–MS. Subsequent investigation into the source of PL in the immunoprecipitated MR1 eluate revealed high signals for the reduced B6 vitamer pyridoxine in the cell culture media, but only trace levels of PL in fetal calf serum (Table 1). Assuming C1R cells are capable of enzymatic vitamer interconversion, the pyridoxine-rich media is the likely source of this ligand. Thus, we conclude that C1R cells can naturally process and present PL via MR1.

Molecular Basis of MR1 Presentation of Vitamin B6-Related Molecules. We established whether these ligands could upregulate cell surface expression of MR1 using the C1R.MR1 cell line (10). As shown in Fig. 2*B*, PL and PLP could upregulate MR1 cell surface expression in a dose-dependent manner. Then, using a fluorescence polarization assay (17) we determined the half-maximal inhibitory concentration (IC_{50}) value of PL, and closely related vitamers, PLP, pyridoxamine (PM), and pyridoxine (PN) (Fig. 2*C*). Neither the negative control [an irrelevant HLA-A2 binding peptide (NLV)] nor PN showed any binding to MR1, while PL and PLP bound with IC_{50} values of ~22 μM and ~50 μM, respectively. For context, the weak agonist, diclofenac binds MR1 with an IC_{50} of 1.5 mM, while 6-FP and 5-OP-RU bind MR1 with IC_{50} values in the nM range. Accordingly, PL and PLP demonstrate moderate binding affinity to MR1.

We then refolded recombinant human MR1 in the presence of either PL or PLP, and explored whether they stabilize the MR1 protein in vitro by thermostability assays (20). Here, we measured the half-maximum melting temperatures (Tm) of MR1- PL/PLP complexes and compared to MR1-5-OP-RU complexes (Fig. 2*D*). MR1-PL/PLP complexes were stable at 37 °C, with Tm ~ 52 to 53 °C, but to a lower thermal stability than MR1-OP-RU (Tm ~ 63 °C).

To gain insight into the molecular basis underpinning the interactions between MR1*01, and PL or PLP we were able to crystallize the MAIT A-F7 TCR-MR1-PLP and TCR-MR1- PL complexes, consistent with other MAIT TCR-MR1 structural reports (15, 16). We determined the structures of TCR-MR1*01-PL and TCR-MR1*01- PLP to a resolution of 2.40 Å and 1.95 Å, respectively (Fig. 3 and *SI Appendix*, Fig. S1 and Table S1). The electron density corresponding to the ligands was unambiguous, permitting detailed analysis of the mode of binding to MR1 (Fig. 3 *A*–*D*). Both ligands occupied the A-pocket of MR1*01, and their aldehyde groups formed Schiff base bonds with the ε-amino group of MR1-Lys43 (Fig. 3 *C* and *D*). Here, the pyridine rings of both vitamers were buried by MR1 and were located centrally within the MR1 A-pocket, positioned toward the base of the β-sheet, exhibiting very limited solvent accessibility. In both structures, the conformations of the side chains for the majority of ligand-contacting residues were conserved (Fig. 3 *E* and *F*), with minimal conformational changes within the pocket, compared to MR1*01-5-OP-RU (Fig. 3*F*). Of note, the MR1*01-Lys43 side chain was displaced by ~1.4 Å in the structures of MR1*01-PL and PLP to accommodate the PL scaffold (Fig. 3 *E*–*G*).

In the MR1*01-PL structure, the pyridine ring was sequestered by hydrophobic interactions within the aromatic cradle of MR1*01, Tyr7, Tyr62, Trp69, and Trp156. In addition, the OH group of the PL formed water-mediated H-bonds with MR1*01-Ser24 and chlorine-based H-bond with Arg 9 of the pocket. The amine group of the PL ligand also formed water-mediated H-bonds with MR1*01-Tyr62 and Trp156. In the structure of MR1*01-PLP, the ligand sits similarly to PL inside the cleft, while the monophosphate ester group PLP formed a network of H-bonds with the three evolutionarily conserved residues of Arg9, Ser24, and Arg94 that protrude up into the cleft. Notably, PLP also formed an extensive network of water-mediated hydrogen bonds with MR1*01-Gln153, Tyr152, and Tyr62. Accordingly, we

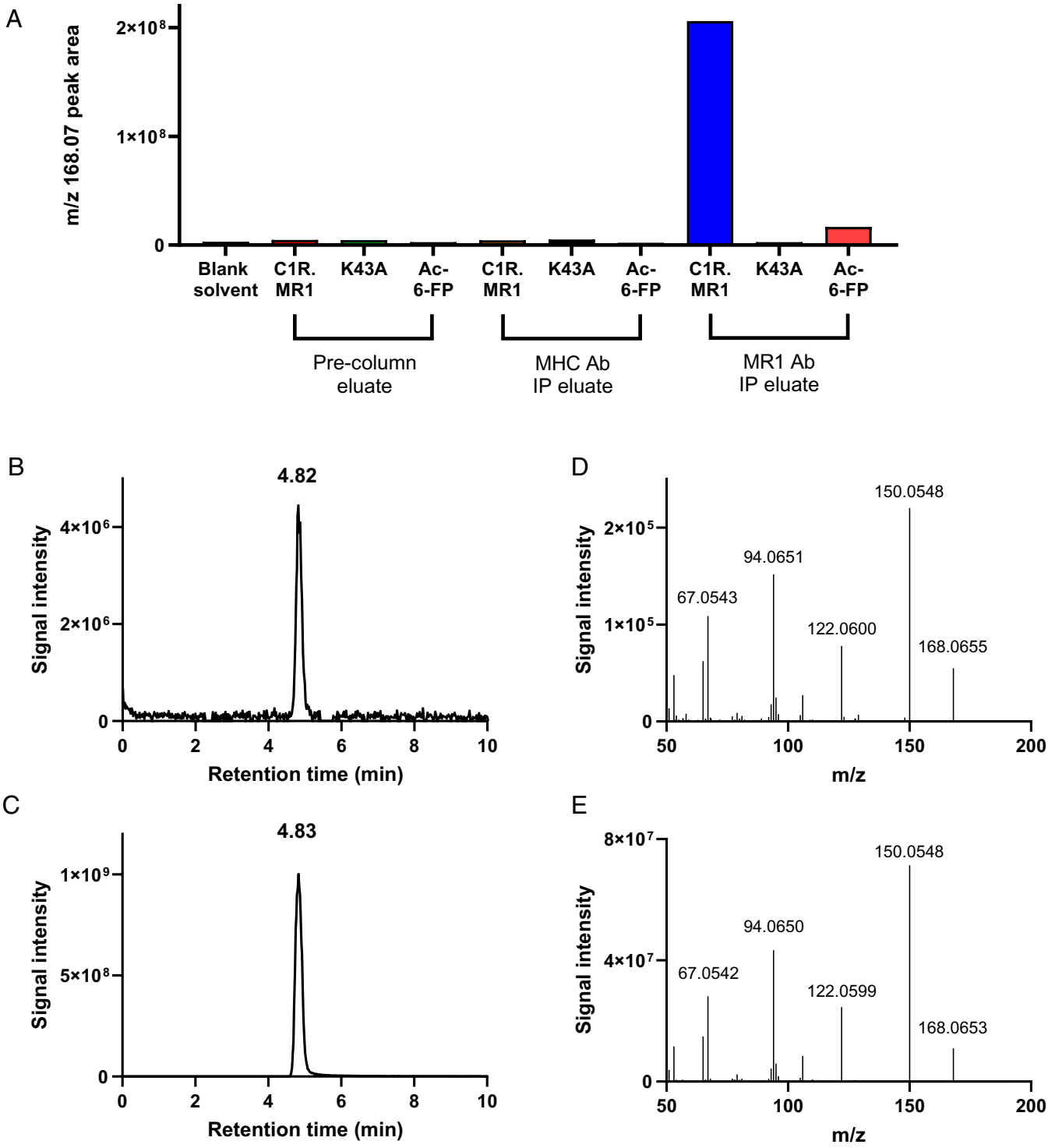

Fig. 1. MR1*01 ligand pyridoxal identified by (*A*) LC–MS signal abundance in the C1R.MR1*01/MR1-IP sample only; and by extracted ion chromatogram comparison for m/z 168.07 in C1R.MR1*01-IP sample (*B*) and PL standard injection (*C*); and MS2 fragmentation of m/z 168.07 in C1R.MR1*01-IP sample (*D*) and pyridoxal standard (*E*).

provide a structural basis of how PL and PLP can be bound and presented by MR1*01.

MR1-Pyridoxal Specifically Activates the 7.G5 TCR. MAIT cells play critical roles in the immune system, particularly in recognizing microbial infections via the recognition of microbial metabolites presented by MR1 (31). The A-F7 TCR is composed of the invariant Vα7.2-Jα33 (TRAV1-2-TRAJ33) α-chain paired with TRBV6-1 (25) and is considered a prototypic MAIT TCR with specificity for riboflavin-based antigens, with 5-OP-RU being the most potent (20). TCR-reporter cells expressing the MAIT A-F7 TCR (Jurkat.MAIT.A-F7) were not activated by PL or PLP in the presence or absence of either C1R cells expressing endogenous levels of MR1*01 or A549 cells (heterozygous expression of MR1*01 and MR1*04), although they were robustly activated by 5-OP-RU (Fig. 4 *A* and *B*). MR1 presentation of PL and PLP in A549 was evident by upregulation of MR1 in the presence of these molecules (*SI Appendix*, Fig. S2*A*).

The 7.G5 TCR (TRAV38-TRAJ31/TRBV25-1) is an MR1 restricted αβTCR capable of specifically targeting a wide range of

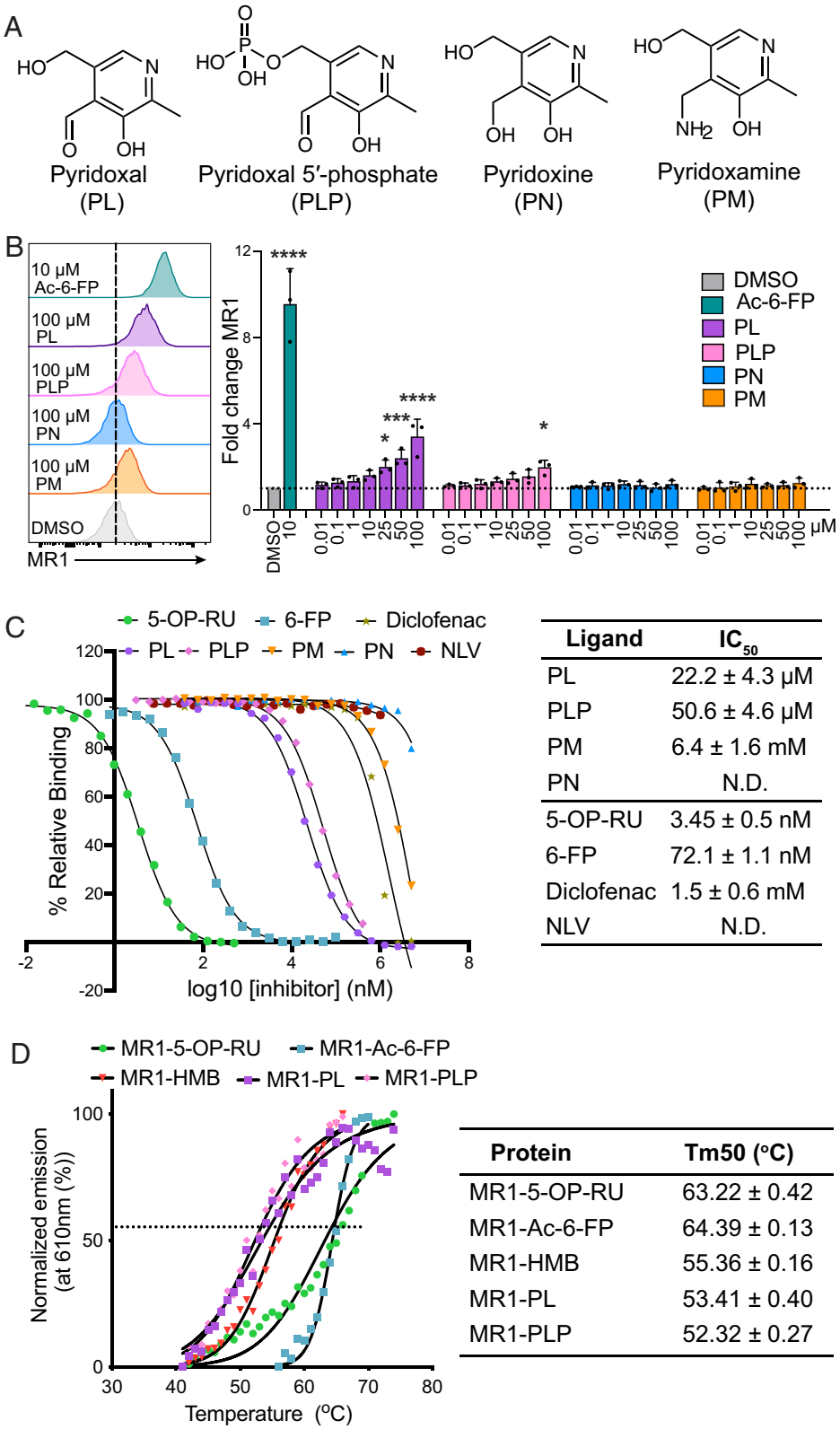

Ligand	IC_{50}
PL	22.2 ± 4.3 μM
PLP	50.6 ± 4.6 μM
PM	6.4 ± 1.6 mM
PN	N.D.
5-OP-RU	3.45 ± 0.5 nM
6-FP	72.1 ± 1.1 nM
Diclofenac	1.5 ± 0.6 mM
NLV	N.D.

Protein	Tm50 (°C)
MR1-5-OP-RU	63.22 ± 0.42
MR1-Ac-6-FP	64.39 ± 0.13
MR1-HMB	55.36 ± 0.16
MR1-PL	53.41 ± 0.40
MR1-PLP	52.32 ± 0.27

Fig. 2. Pyridoxal scaffolds bind to MR1*01. (*A*) Chemical structures of various vitamin B6 molecules. (*B*) Cell surface expression of MR1*01 on C1R.MR1 cells (measured as mean fluorescence intensity, MFI) in response to 3 h incubation with Ac-6-FP and vitamin B6 compounds at the indicated doses. DMSO was the vehicle control for all compounds. The dotted line shows the geometric MFI value of DMSO. Data show fold increases over background intensity (mean ± SEM from 2 independent experiments). (*C*) Affinity measurement of the vitamin B6 compounds binding to MR1*01 determined using a fluorescence polarization assay. IC_{50} values were determined from two independent experiments performed in triplicate. Mean values are plotted with SD represented in error bars. (*D*) Thermostability of soluble MR1*01-antigen (Ag) complexes measured by fluorescence-based thermal shift assay with mean Tm_{50} across three independent experiments, each in triplicate.

cancer cells (23), and subsequently some noncancerous cells were also demonstrated to be targets for T cells expressing this TCR (24). To assess whether PL ligands were able to activate responses via the 7.G5 TCR we used SKW3 cells that overexpress the human CD8αβ coreceptor known to bind MR1 (32) and the 7.G5 TCR, reproducing the CD8-expression of the primary 7.G5 T cell clone (23). These SKW3 cells also express endogenous MR1*01 (*SI Appendix*, Fig. S2 *B* and *C*) and were activated by PL in the absence of additional antigen-presenting cells in a titratable manner as measured by increased CD69 expression (Fig. 4*C*). The addition of PLP activated 7.G5 SKW3 reporter cells to a lesser extent at higher concentrations (10 and 100 μM), suggesting PLP may be a weaker activator, or that it requires conversion to the activating ligand. Blocking by the αMR1 antibody, 8F2.F9, or Ac-6-FP competition for MR1 occupancy, support the MR1 dependence of this activation (Fig. 4 *E* and *F* and *SI Appendix*,

Table 1. Detection of PL and PN in healthy primary, immortalized and actively cancerous cell lines

			pmol vitamer/mg cell pellet	
Cell line name	Description	Cell line category	PL	PN
PBMC donor 1	Peripheral blood mononuclear cells (PBMCs)	Primary/healthy	0.046	–
PBMC donor 2			0.182	0.201
PBMC donor 3			0.092	0.094
Splenocyte donor 1	Splenocytes		0.026	–
Splenocyte donor 2			0.058	–
Splenocyte donor 3			0.017	–
1106 K	Epithelial keratinocytes from human skin	Immortalized	0.061	–
K562	Lymphoblast cells isolated from chronic myelogenous leukemia patient	Immortalized/cancerous	0.280	0.755
MDA-MB-231	Breast cancer cell line		0.463	1.190
THP1	Monocyte from acute myeloid leukemia patient		0.809	–
VMM1	Melanoma cell line		0.146	–
A549	Lung carcinoma epithelial cells		0.868	2.067
Media component	Description		Media concentration (nM)	
Fetal calf serum	Cell culture media supplement	NA	12.5 ± 0.7	–
RF10	Supplemented RPMI base media	NA	1.8 ± 0.2	797 ± 33

Expressed as pmol of vitamer per mg of cell pellet (wet weight); – denotes not detected.

Fig. S3*A*). The response was also dependent on the expression of the 7.G5 TCR, such that SKW3.CD8αβ.GIL (expressing an HLA-A*02:01 restricted TCR specific for the influenza $M_{58–66}$ peptide) was unresponsive to both PL and PLP (*SI Appendix*, Fig. S3*B*). As per the original description of the 7.G5 TCR, SKW3.CD8αβ.7.G5 showed higher activation when incubated with A549 cells as the APC (MR1*01/04 heterozygous (24)) compared to A549.β_2m^{ko} (Fig. 4*D*). This activation was abrogated by addition of 10 μM Ac-6-FP, consistent with MR1 ligand-dependent activation (Fig. 4 *E* and *F*).

Enhanced Activation of 7.G5 by APC Overexpressing MR1 Containing the Arg9His Substitution. MR1 polymorphisms have the potential to impact on Ag presentation, particularly

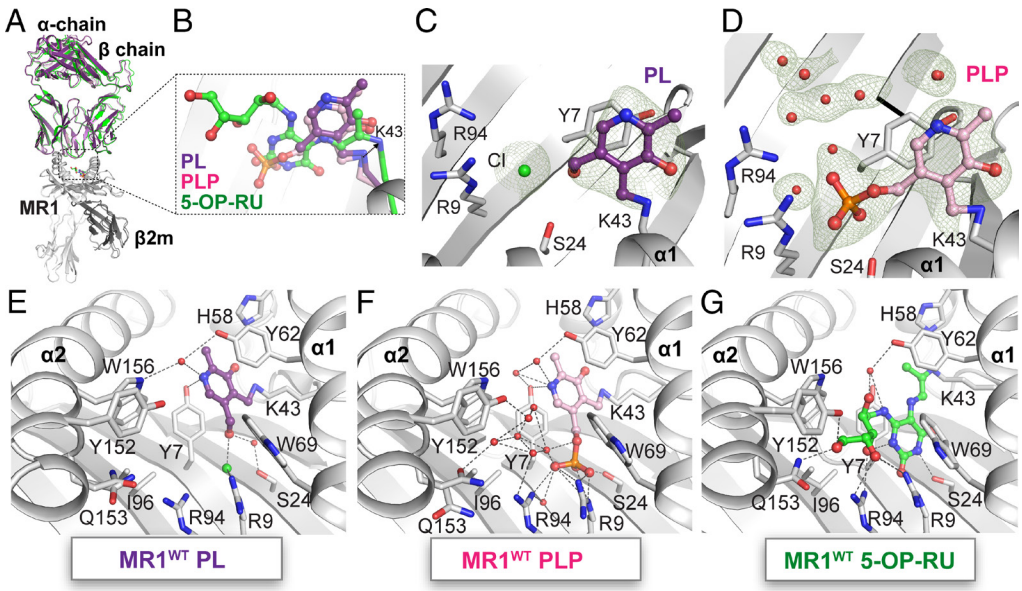

Fig. 3. Crystal structures of MR1*01 with Vitamin B6 ligands. (*A*) The overall topology of the A-F7 TCR-MR1*01-PL, -PLP, and -5-OP-RU (PDB ID: 6PUC) crystal structures. (*B*) Superposition of MR1*01-PL, PLP, and 5-OP-RU metabolites within the binding cleft, showing the K43-Ag Schiff base interaction. Omit maps contoured at 3σ (Fo − Fc map; green mesh) of pyridoxal (*C*) and PLP (*D*) after stimulated annealing refinements in Phenix crystallography package. The interactions between the PL (*E*), and PLP (*F*), and 5-OP-RU (PDB; 6PUC) (*G*), and the residues of A pocket in the MR1-Ag structures, highlighting small conformational differences of MR1*01 residues between various structures. MR1*01 and β2-microglobulin (β2m) were colored white and gray, respectively. The ligands were colored as follows: PL, purple; PLP, pink; and 5-OP-RU, green. Red spheres denote water molecules, green spheres are chloride ions.

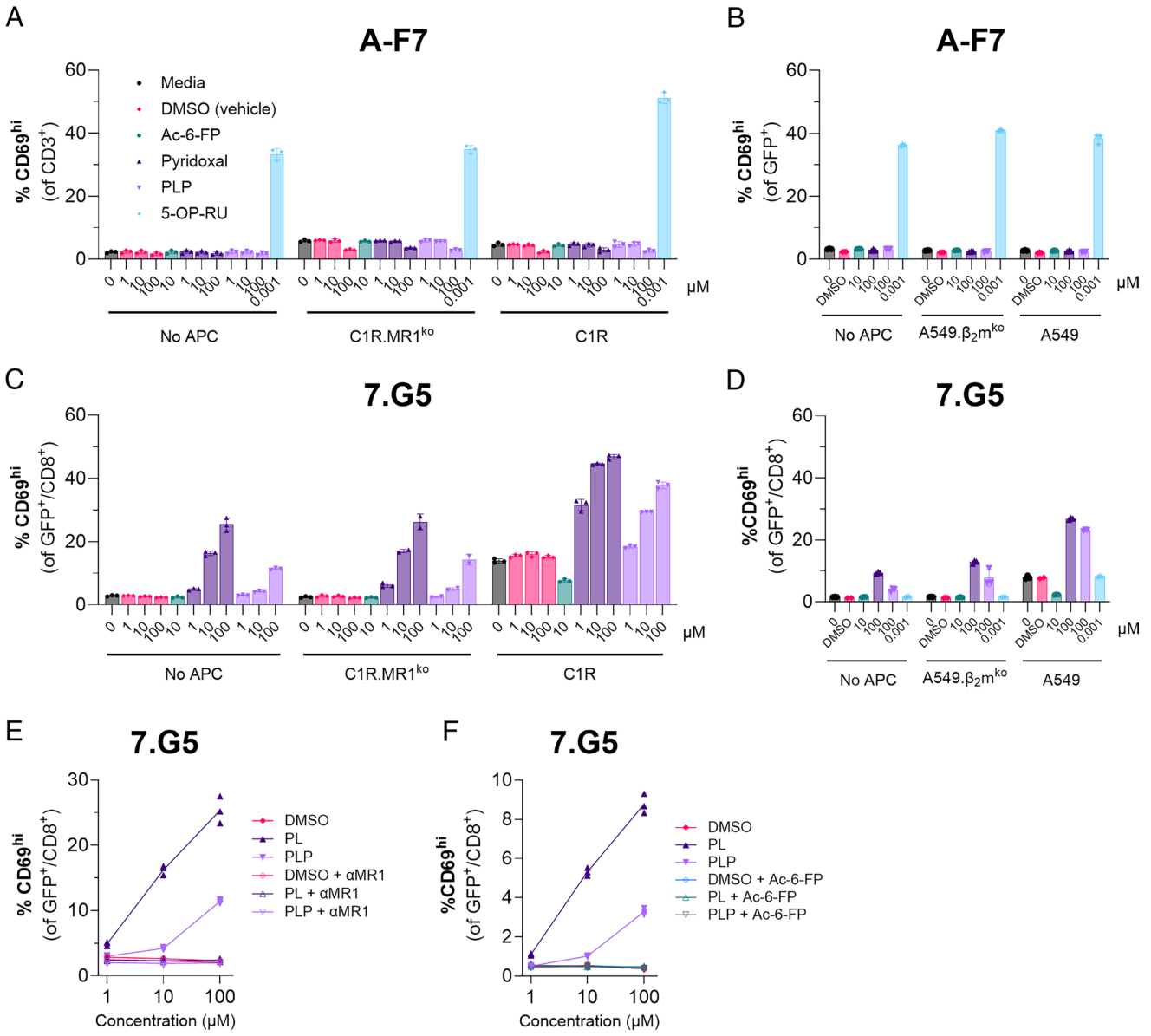

Fig. 4. Pyridoxal and PLP differentially activate T cell reporter lines expressing the A-F7 and 7.G5 TCRs. SKW3/Jurkat activation was assessed by flow cytometry staining for CD69 upregulation after overnight stimulation, reported as a % of SKW3/Jurkat reporter cells expressing high levels of CD69 (see *SI Appendix*, Fig. S4 for gating strategy). (*A*) Jurkat.MAIT.A-F7 were stimulated alone (No APC) or with C1R.MR1ko or C1R expressing endogenous levels of MR1*01 at a 2:1 responder:stimulator ratio and in the presence of media alone, 10 μM Ac-6-FP, 1 to 100 μM PL, 1 to 100 μM PLP, DMSO equivalent to the PL/PLP vehicle, or 1 nM 5-OP-RU. Note this assay was performed in folate-containing media; all subsequent assays were performed in folate free media. (*B*) Jurkat.MAIT.A-F7 were stimulated alone (No APC) or with A549 or A549.β_2m^{ko} (5:1 responder:stimulator ratio) in the presence of media alone, 10 μM Ac-6-FP, 100 μM PL, 100 μM PLP, DMSO equivalent to the PL/PLP vehicle or 1 nM 5-OP-RU. (*C* and *D*) SKW3.CD8αβ.7.G5 were stimulated as in *A* and *B*. (*E* and *F*) SKW3.hCD8αβ.7.G5 were incubated overnight in the presence of 1 to 100 μM PL, PLP, or DMSO equivalent to the PL/PLP vehicle, either (*E*) with or without antibody blocking using the 8F2.F9 (αMR1) antibody or (*F*) with or without competition from 10 μM Ac-6-FP. Graphs show technical triplicates in single experiments, bars in *A*–*D*, and lines in *E* and *F* are means, error bars are SD.

the Arg9His substitution found in the MR1 Ag-binding cleft of MR1*04 allomorphs (7). We first tested whether PL upregulated surface expression of the $MR1^{R9H}$ molecule on C1R cells. As expected, PL, and, to a lesser extent PLP, upregulated MR1 surface expression of MR1*01 ($MR1^{WT}$) on overexpressing C1R cells in a dose-dependent manner, albeit less effectively than equivalently dosed Ac-6-FP (Fig. 5*A*). C1R cells overexpressing $MR1^{R9H}$, pulsed with PL showed MR1 upregulation comparable to Ac-6-FP, and greater than PLP (Fig. 5*A*), suggesting $MR1^{R9H}$ (and by extension MR1*04) may preferentially bind and present PL on the cell surface. We noted a modest induction of surface $MR1^{R9H}$ expression with a high dose of pyridoxamine, despite weak binding of pyridoxamine to MR1*01 measured by fluorescence polarization (Fig. 2*C*), possibly due to conversion of the vitamer to pyridoxal or PLP by the cells. We next examined the capacity for $MR1^{R9H}$ to activate β_2m^{null} 7.G5 reporter T cells (SKW3.β_2m^{null}.hCD8αβ.7.G5) which lack capacity for self-presentation via MR1. Notably, APCs solely expressing $MR1^{R9H}$ activated reporter T cells expressing the 7.G5 TCR significantly greater than APC overexpressing MR1*01 ($MR1^{WT}$) and parental C1R cells. In contrast, no appreciable response was detected by 7.G5 reporter cells toward $MR1^{K43A}$ overexpressing cells (Fig. 5*B*) consistent with the earlier Ag elution experiments (Fig. 1).

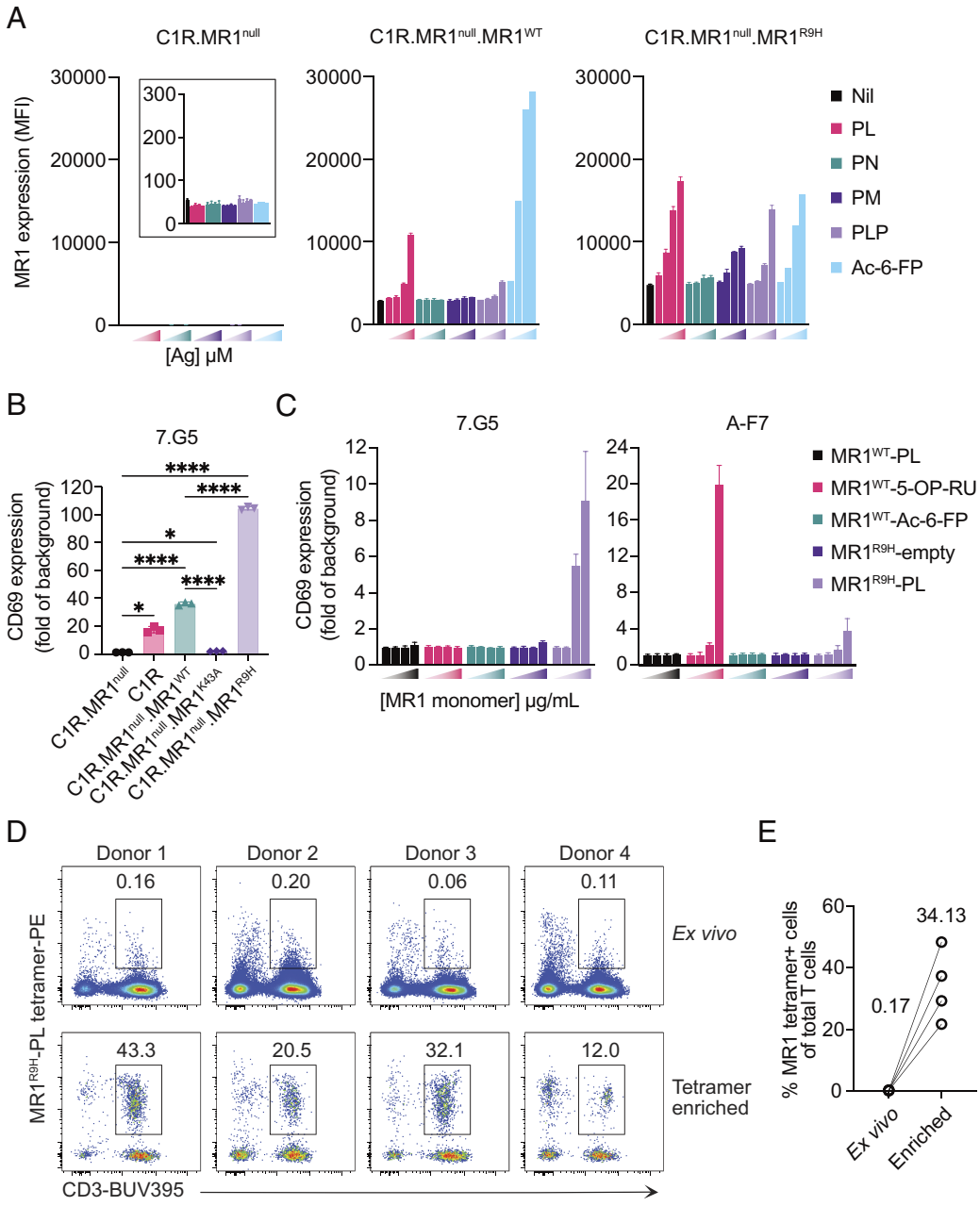

Fig. 5. Pyridoxal is preferentially presented by MR1*04 for recognition by 7.G5 and other MR1-reactive T cells. (*A*) MR1 upregulation of MR1 deficient ($MR1^{null}$), MR1*01 ($MR1^{WT}$), or MR1*04 ($MR1^{R9H}$) overexpressing C1R cells incubated overnight with B6 vitamers or Ac-6-FP titrated 10-fold from 200 μM. (*B*) CD69 upregulation (median fluorescence intensity; fold change of T cells alone) of 7.G5 reporter SKW-3 cells cultured overnight 3:1 with parental C1R cells or genetically engineered C1R cells described above using media supplemented with folate. (*C*) CD69 upregulation (median fluorescence intensity; fold change of T cell alone) of 7.G5 or A-F7 reporter SKW-3 cells stimulated with plate-bound MR1 titrated 5-fold from 50 μg/mL. (*D*) $MR1^{R9H}$-pyridoxal tetramer staining of primary T cells directly (ex vivo) or after enrichment (tetramer enriched) from healthy donor blood. (*E*) Pairwise frequencies of $MR1^{R9H}$-pyridoxal tetramer positive T cells as a percentage of total T cells before (ex vivo) and after (enriched) tetramer enrichment with mean values displayed. (*A*–*C*) Data are representative of two independent experiments performed in triplicate. Mean values and error bars (SD) are displayed. Statistical significance was determined using a one-way ANOVA with the Geisser-Greenhouse correction and Tukey's multiple comparison test where *$P < 0.05$, ****$P < 0.0001$. (*D* and *E*) Data are from one experiment.

To further determine whether PL is presented by $MR1^{R9H}$ to the 7.G5 TCR we performed an in vitro plate-bound antigen assay. Soluble $MR1^{R9H}$ protein was refolded with or without PL, as well as control MR1*01-antigen complexes to stimulate 7.G5 or control A-F7 reporter T cells (β_2m^{null}) directly. We immobilized titrating concentrations of soluble MR1 on a microplate and overlaid the reporter T cells (Fig. 5*C*). Activation of 7.G5 to "plate-bound" $MR1^{R9H}$-PL confirmed efficient presentation by MR1*04 for recognition by the 7.G5 TCR. Interestingly, we observed weak activation of control A-F7 cells by high concentrations of MR1*04-PL, despite the lack of detectable activation by APC expressing this allomorph (Fig. 4*B*). This finding highlights potential antigen promiscuity that has been observed for some MAIT clones (19, 33). Activation of the 7.G5 TCR by plate-bound MR1*01-PL monomer was not detectable (Fig. 5*C*), reflecting differences in the sensitivity of the cell-based and plate-based activation methods.

To generalize our findings beyond the 7.G5 reporter T cell line, we stained PBMCs with $MR1^{R9H}$-PL tetramers to determine whether MR1*04-PL-reactive T cells were present in healthy blood donors (Fig. 5 *D*, *Upper* panel). The ex vivo frequency of tetramer positive cells as a proportion of total T cells was low, with a mean value of 0.17% (Fig. 5*E*), and similar to previously reported target-specific circulating MR1-reactive T cells (22). To further interrogate this population of $MR1^{R9H}$-PL-reactive T cells, we

used tetramer-specific magnetic enrichment to partially purify the tetramer-bound T cells (Fig. 5 *D*, *Lower* panel). We observed a substantial enrichment of tetramer positive T cells from all donors (Fig. 5*E*), suggesting broad recognition of MR1 presenting pyridoxal by circulating T cells. We next addressed the previously reported cancer specificity of 7.G5 T cell recognition (23) by examining levels of PN-uptake by cancer cells and healthy primary human PBMCs and splenocytes and subsequent conversion to PL within these cells using a metabolomics approach (Table 1). Strikingly, the cancer cells showed up to 50-fold higher levels of intracellular PN than the primary cells despite being cultured in the same cell culture media.

Discussion

Our understanding of the ligand binding characteristics of MR1 has mostly revolved around riboflavin-related molecules based on the original description of MR1 binding to 6-formylpterin, a folic acid (vitamin B9) metabolite, and metabolites that originate from bacterial riboflavin (vitamin B2) biosynthesis pathways (10). Various compounds based around the core pterin and uracil structures of these molecules have been shown to bind MR1 and variably activate MAIT cells and other MR1-restricted T cells (12, 20, 34). Using a structural informatics approach, we have also shown broader binding of a range of diverse chemical scaffolds that bind MR1, including a range of pharmaceutical drugs and other small molecules (16). These and other studies (13, 14) highlight the capacity for a more diverse range of MR1 ligands; however, studies of naturally presented ligands remain limited. Thus, we developed an unbiased ligandomics approach for studying MR1-bound metabolites based on affinity purification of solubilized membranal MR1 complexes and LC–MS analysis of the eluted material. Importantly we incorporated a series of controls to identify and exclude chemical noise, generating more confidence in the remaining ligand candidate signals. Here, we report that two vitamin B6 metabolites, PL and its phosphorylated derivative PLP, have the ability to bind and upregulate cell surface MR1 while structural studies showed that both ligands formed a Schiff base covalent bond with MR1 through positioning in the A-pocket.

The MAIT TCR A-F7 was not readily activated by PL or PLP in the context of MR1*01, consistent with lack of direct contact of this ligand with the MAIT TCR in the crystal structures where A-F7 was used as a crystallization aide. We considered whether these ligands could be antigens for non-MAIT MR1-reactive T cells that express more diverse TCRs and as such can exhibit specificity differences compared to that of most MAIT cells. Arguably, one of the most "prominent" MR1 restricted T cell clones to be characterized was that of the reported "pan cancer" T cell clone, 7.G5. Specifically, 7.G5, initially reported to be nonreactive to healthy cells, was activated by a broad range of tumor cell lines, lysed tumor cells, and promoted anti-tumor immunity in a MR1-dependent, ligand-dependent manner (23). However, the MR1-bound ligand for the 7.G5 TCR was unknown. Thus, we examined the reactivity of the 7.G5 TCR toward MR1-PL and PLP complexes using cell-based assays. Noting the uncertainty around the pan-tumor specificity of this TCR (23, 24), the nature of the Ag presented to 7.G5 is crucial to fully understand target cell specificity. We demonstrated dose-dependent recognition of PL and to a lesser extent PLP by 7.G5 reporter cells. Since PL is central to many biochemical processes, this finding immediately suggests a mechanism of differential cell recognition through sensing distinct metabolic profiles. Previous observations have also suggested that 7.G5 preferentially recognizes the MR1*04 allotype (24). We also observed an enhanced endogenous response to cells expressing the Arg9His polymorphism found in MR1*04 and our findings demonstrate preferential presentation of PL by this allomorph.

Pyridoxal is one form (vitamer) of the essential vitamin B6 that is present in all cells. Underpinned by its ability to form Schiff bases, it is arguably one of the most versatile organic cofactors in biology, and is involved in over 140 different enzymatic activities (35). However, there is considerable evidence that cancer cells preferentially take up this molecule from the extracellular milieu and that higher systemic PL levels may offer some protection against cancer (36–41). Other studies have suggested that this preferential uptake of vitamin B6 vitamers may promote tumorigenesis by depriving infiltrating T cells of this vital molecule in a manner akin to tryptophan depletion in the tumor microenvironment (TME) (42–44). Moreover, PL metabolites have been shown to be cancer-specific biomarkers (38, 40, 45–48). Using our LC–MS based metabolite identification workflows we examined the levels of PL and PN in cancer cell lines compared to primary cells and demonstrated up to 50-fold increases in intracellular PL in cancer cells. This reflects the enhanced metabolism of the cancer cells and also suggests that cancer cells may present higher levels of PL in complex with MR1 in cancer cell lines, consistent with the observations of Crowther et al. (23). This MR1-recognition of cancer cells may represent a tightly controlled axis of cancer immunosurveillance whereby higher levels of PL in these cells is communicated to MR1-restricted T cells facilitating preferential recognition of the cancer. Targeting nonclassical MHC and MHC-I-like molecules remains relatively unexplored but may represent an alternative approach for cell-based immunotherapies and biotherapeutic development.

Materials and Methods

Small Molecules and Peptides. The compound 5-OP-RU was synthesized as a solution in DMSO as described previously (11) and its concentration quantified by NMR spectroscopy (49). 6-FP and Ac-6-FP were purchased from Schircks Laboratories (Switzerland). Vitamin B6 was purchased from Sigma and dissolved in DMSO, water, or 1 M HCl for cellular assays. The control influenza A $M1_{58-66}$ epitope (peptide sequence GILGFVFTL, >90% purity) was synthesized using standard Fmoc chemistry by Mimotopes Australia.

Generation of Cell Pellets for MR1 Immunoprecipitation. C1R.MR1, C1R.$MR1^{K43A}$ were grown to high density in RF5 media (RPMI 1640 (Gibco) supplemented with 2 mM MEM nonessential amino acid solution (Gibco), 5 mM HEPES (Sigma-Aldrich), 2 mM L-glutamine (Gibco), Pen Strep [100 U/mL Penicillin 100 μg/mL streptomycin] (Gibco), 50 μM 2-mercaptoethanol (Sigma-Aldrich) and 5 % heat inactivated fetal calf serum) in Corning 1.7 L roller bottles at 37 °C, 5% CO_2. For Ac-6-FP treated cells, Ac-6-FP was added to a final concentration of 1 μM for the last 19.5 h of culture. To harvest cells, culture was centrifuged in 500 mL V-bottom corning tubes at 1,450×*g*, 4 °C for 10 min, supernatant discarded, and the pellets washed twice by resuspension in phosphate-buffered saline (PBS) and similar centrifugation. Washed cells were snap frozen and stored at −80 °C until use.

Immunoprecipitation. 8F2.F9 (anti-MR1) and W3/62 (anti-MHC-I) antibodies were separately cross-linked to protein G agarose as described previously (50). Cell pellets generated from C1R.MR1*01, C1R.MR1*01.K43A, and C1R.MR1*01/Ac-6-FP incubation (1.1e9, 4.6e8, and 8.6e8 cells, respectively) were lysed via cryo-milling and subsequent incubation in lysis buffer (0.5% IGEPAL 630, 50 mM TRIS (pH 8.0), 150 mM NaCl, and 1× Complete protease inhibitor cocktail; Roche) for 45 min at 4 °C, prior to clearing by centrifugation and ultracentrifugation as described previously (50). These final supernatants were flowed through 3 successive prepared columns: 1) A precolumn containing protein G agarose beads containing no antibody, 2) W6/32 Ab-linked protein G agarose, and 3) 8F2.F9 Ab-linked protein G agarose. All three columns were then separated and subjected to the following washes: 20 CV of wash buffer 1 (0.005% IGEPAL, 50 mM TRIS pH 8, 150 mM NaCl, 5 mM EDTA, 100 μM PMSF, 1 μg/mL

Pepstatin A in MilliQ water); 20 V of wash buffer 2 (50 mM TRIS pH 8, 150 mM NaCl in MilliQ water); 20 CV of wash buffer 3 (50 mM TRIS pH 8, 450 mM NaCl in MilliQ water); and finally wash buffer 4 (50 mM TRIS pH 8 in MilliQ water). The resin/TRIS buffer was then transferred to 1.5 mL low-bind Eppendorf tubes, and briefly centrifuged to collect beads and remove the buffer. The beads were resuspended in 1 mL of optima water, briefly mixed, and again centrifuged to discard supernatant. This wash was repeated for total of three times, before finally boiling at 90 °C for 10 min to dissociate immunoprecipitated proteins and their ligands from agarose beads, before centrifugation at 13,000 rcf for 10 min to remove final supernatant as the IP eluate. Eluates were aliquoted and stored at −80 °C until further analysis by LC–MS.

LC–MS Analysis. IP eluate aliquots (150 μL) were prepared by a 3:1 protein precipitation with acetonitrile containing 0.1% formic acid. Samples were left to sit at room temperature for 10 min before centrifugation at 15,000 rcf to precipitate any MR1 or MHC proteins, while simultaneously liberating any previously bound ligands into the supernatant. Supernatant was transferred to LC–MS vials for analysis on a Thermo Q-Exactive Plus Orbitrap mass spectrometer coupled to a Thermo UltiMate 3000 UPLC system fitted with an iHILIC®-(P) Classic, HILIC Column (150 × 4.6 mm, 5 μm, 200 Å) column. Mobile phases A (pure acetonitrile) and B (20 mM ammonium carbonate, pH 10) were shifted from 20 to 50% B over 15 min, from 50 to 95% B from 15 to 18 min, held for 3 min at 95% B before re-equilibrating at 20% B from 24 to 32 min. The flow rate was 0.5 mL/min and the column temperature was set to 25 °C. All samples were injected in both positive and negative mode, with 140,000 MS1 resolution and a scan range from 80 to 800 m/z. DDA for fragmentation was triggered by an AGC target of 8e3 ions for up to 10 precursors per experiment cycle. To minimize fragmentation of background ions, the Apex Trigger function was used (5 to 60 s window), dynamic exclusion was set to 10 s and only singly or doubly charged ions were permitted for selection. To obtain informative MS2 spectra across potentially wide range of molecular structures, collision energy was stepped at 20, 40, and 60 eV.

Ligand Identification. Immunoaffinity-purification of any target protein is an effective enriching technique, but thousands of unrelated chemical compounds inevitably remain in any given experiment, due nonspecific binding to materials used in the procedure. To deal with this complexity, elutions from a protein-G precolumn and a non-MR1 antibody (W6/32), of the three key sample lysates (C1R.MR1*01, C1R.MR1*01.K43A, and C1R.MR1*01/Ac-6-FP) were all collected and analyzed by LC–MS, alongside the samples of interest. Any compounds appearing in precolumn or control antibody immunoprecipitations were considered to represent metabolites engaging in nonspecific interaction with the immunoaffinity-purification procedure, and were discounted from any ligand searching analysis.

To facilitate signal sorting along these lines, raw data files were imported into MS-DIAL, and signals which were present in the C1R.MR1/8F2F9 pull-down but absent or very low in all other samples were selected for further consideration. These candidate signals were further interrogated by assessing retention time, peak shape, signal-to-noise ratio, DDA triggered MS2 acquisition, and spectral fingerprint matching within MS-DIAL, against a library downloaded from the MassBank of North America (MoNA) (29). Only a small number of signals were shortlisted to this point, some of which are still under investigation. The extracted ion chromatogram for m/z 168.07 met all the above-described criterion and appeared to match the fragmentation pattern for PL stored in the Mass bank of North America, as analyzed in MS-DIAL. Raw MS1 and MS2 spectra for the m/z 168.07 signal were then imported into SIRIUS 4.0 as an orthogonal identification strategy, where pyridoxal appeared as the highest ranking compound explaining the queried spectra, with a CSI:FingerID score of −36.423. Following up on this, a PL standard (10 μM, 80% ACN) was purchased and injected into the same LC–MS system described above, for full confirmation of correct molecular identification.

Cell Lines and Tissues. C1R, SKW-3, and Jurkat derived cell lines were maintained in RF10 [RPMI 1640 (Gibco) supplemented with 2 mM MEM nonessential amino acid solution (Gibco), 5 mM HEPES (Sigma-Aldrich), 2 mM L-glutamine (Gibco), Pen Strep [100 U/mL Penicillin 100 μg/mL streptomycin] (Gibco), 50 μM 2-mercaptoethanol (Sigma-Aldrich) and 10 % heat inactivated fetal calf serum]. A549 derived cell lines were maintained in DMEM10 (DMEM [low glucose, pyruvate] (Gibco), supplemented as for RF10). All lines were cultured at 37 °C, 5% CO_2.

C1R.MR1 and C1R.MR1^{null}.MR1 cells (32) overexpress MR1*01 (51), while C1R.MR1^{R9H} and C1R.MR1^{null}.MR1^{R9H} or C1R.MR1^{K43A} and C1R.MR1^{null}.MR1^{K43A} cells overexpress MR1 with substitutions of Arg9His and Lys43Ala in the mature MR1, respectively (7). All MR1 overexpressing cells are GFP^{+}. C1R.A*02:01 have been engineered to overexpress HLA-A*02:01, under hygromycin selection (52). Jurkat.MAIT.A-F7 and SKW-3.β_2m^{null}.A-F7 express a TRAV1-2–TRBV6-1 MAIT TCR (20).

C1R.MR1^{ko} and A549.β_2m^{ko} were generated via transfection of C1R/A549 with pSpCas9(BB)-2A-GFP (PX458) plasmid (53) containing guide RNA selected using CHOPCHOP (54) to target MR1 (chr1:181049205, guide 5′ AGAACCTCGCGCCTGATCAC 3′) or β_2m (chr15:44715428, guide 5′ CGTGAGTAAACCTGAATCTT 3′), respectively. pSpCas9(BB)-2A-GFP (PX458) was a gift from Feng Zhang (Addgene plasmid # 48138). Cells were bulk sorted by flow cytometry for transient GFP expression, and clones generated by subsequent limiting dilution (C1R.MR1^{ko}) or single cell sorting based on negative cell surface expression of MHCI (A549.β_2m^{ko}). C1R.MR1^{ko} clones were selected based on lack of MR1 surface upregulation on overnight induction with 20 μM Ac-6-FP detected by flow cytometry after staining for MR1 using the 8F2.F9 antibody (in-house production) and APC-conjugated F(ab′)2-Goat anti-Mouse IgG (H+L) Secondary Antibody (eBioscience), and verified by genomic sequencing of the targeted region of MR1. A549.β_2m^{ko} were selected based on lack of MHCI surface expression detected by staining with W6/32 (in-house production) and PE conjugated F(ab′)2-Goat anti-Mouse IgG (H+L) Secondary Antibody (SouthernBioTech, cat#1032-09) and verified by genomic sequencing of the targeted region of β_2m.

Coexpression of the 7.G5 and A-F7 TCR α and β chains (23) in SKW3.hCD8αβ.7.G5 or SKW3.β_2m^{null}.hCD8αβ.7.G5 cells was achieved by retroviral transduction of SKW3.hCD8αβ or SKW3.β_2m^{null}.hCD8αβ cells with a pMIG plasmid encoding the cDNA of relevant TCR α and β chains and utilizing a 2 A self-cleaving peptide linker as described previously (51). Cells were sorted for high CD3 and GFP expression by flow cytometry after staining with anti-CD3-PE-Cy7. SKW3.hCD8αβ.GIL were similarly generated to express an αβ TCR specific for the immunodominant HLA-A*02:01 restricted influenza A M1$_{58-66}$ epitope (sequence GILGFVFTL). The expressed TCR is TRAV27*01-TRAJ42*01(CDR3 CAGAEGGSQGNLIF), TRBV19*01-TRBJ2-2*01 (CDR3 CASSIRSTGELFF) and was selected via the VDJdb (https://vdjdb.cdr3.net) (55) and originally identified by Grant et al. (56). SKW3.hCD8αβ are derived from the SKW-3 T cell line from the DSMZ-German Collection of Microorganisms and Cell Cultures (Braunschweig, Germany) and sequentially engineered to overexpress human CD8αβ.

CD69 Activation Assays. For SKW3 activation assays, both antigen-presenting cells (C1R and A549 derivatives) and responders (SKW3 and Jurkat lines) were washed twice in PBS to remove folate from the culture media prior to conducting the assay in folate free media [RPMI 1640 Medium [no folic acid] (Gibco) supplemented with 10 % fetal calf serum, 1× GlutaMAX™ (Gibco), Pen Strep [100 U/mL Penicillin 100 μg/mL streptomycin] (Gibco), 1 mM HEPES (Gibco) and 1× MEM nonessential amino acids (Gibco)] unless otherwise stated. For stimulation with C1R derived cell lines, 5 × 10^4 C1R derivatives were incubated for 1 h with two times the final concentration of the test molecule (PL/PLP/Ac-6-FP/ GILGFVFTL peptide), DMSO equivalent to the vehicle for PL/PLP, or media alone in 100 μL in a 96-well round bottom tissue culture plate (Corning). 10^5 or 1.5 × 10^5 SKW3 responders were then added (2:1 or 3:1 responder:stimulator ratio) in 100 μL. For antibody blocking in the absence of added antigen-presenting cells, 8F2.F9 (αMR1, mouse IgG1, κ), W6/32 (αMHCI, mouse IgG2a, κ), or 9E10 (αmyc, mouse IgG1, κ) (all produced and purified in house and stored in PBS), or equivalent PBS, was added to the SKW3 at 20 μg/mL in folate free media prior to addition of 10^5 SKW3 to 2× concentrated test molecule at a 1:1(v/v) ratio (final 10 μg/mL 8F2.F9). For Ac-6-FP competition assays, 10^5 SKW3 were added to a mix of the test molecule and Ac-6-FP to give a final concentration of 1 to 100 μM test molecule (or DMSO equivalent) and 10 μM Ac-6-FP. For stimulation with A549 derived cell lines, 2 × 10^4 A549/A549.β_2m^{ko} were plated in 100 μL folate free media in a TPP 96-well flat bottom tissue culture test plate in the presence of the 1× concentrated test molecule/DMSO vehicle/media alone and allowed to adhere over 6 h (37 °C, 5% CO_2). The media were then replaced with fresh 100 μL 2× concentrated test molecule/DMSO vehicle/media alone, prior to addition of 10^5 SKW3 in 100 μL. Activation was allowed to proceed overnight at 37 °C, 5% CO_2 (14 to 18 h), prior to staining with BD™ APC Mouse Anti-Human CD69 (Clone L78), BD Pharmingen™ PE-Cy™7 Mouse Anti-Human CD3 (Clone SK7), BD Pharmingen™ PerCP-Cy™5.5 Mouse Anti-Human CD8 (Clone SK1) and LIVE/DEAD™ Fixable Aqua Dead Cell Stain (Invitrogen) in PBS for 30 min (4 °C, dark). Cells were washed with PBS and

fixed with 1% paraformaldehyde in PBS (20 min, room temperature, dark), prior to washing in PBS and acquisition on a BD LSRII flow cytometer using BD FACS Diva software. Data were analyzed using FlowJo v10 (BD) and Graphpad Prism.

For plate-bound MR1 activation assays, titrating concentrations of soluble MR1 monomer in PBS were immobilized onto a 96-well microtiter plate in 50 μL PBS per well and incubated overnight at 4 °C. The following day, unbound MR1 monomer was removed by washing each well three times with 200 μL PBS. 1.5×10^5 SKW-3.β_2m^{null}.hCD8αβ.7.G5 or A-F7 reporter T cell lines were added to each well in 200 μL of RF10 and incubated overnight at 37 °C, 5% CO_2. After stimulation, T cells were harvested and stained with anti-CD3-BUV395 (563546, UCHT1; BD Horizon), anti-CD69-PE (555531, FN50; BD Pharmingen), and a fixable viability dye (eFluor780, 65-0865-18; eBioscience) diluted in PBS + 2% FCS for 20 min at 4 °C. Stained T cells were washed and resuspended in PBS + 2% FCS for acquisition on a BD LSRFortessa.

MR1 Upregulation Assays. As for CD69 assays, all cells were washed twice in PBS prior to conducting the assay in folate free media. For SKW3.hCD8αβ.7.G5 MR1 upregulation assays, 10^5 cells were incubated overnight with test molecules/DMSO vehicle/media alone in a 96-well round bottom tissue culture plate (Corning). For A549 derivatives, 5×10^5 cells were incubated with test molecules/DMSO vehicle/media alone in 1 mL in a well of a 12-well tissue culture plate. After ~26 h A549 were harvested with TrypLE™ Express Enzyme (Gibco) for staining. Cells were stained with 10 μg/mL 8F2.F9 antibody in PBS (30 min, 4 °C, dark). Cells were washed twice with PBS, then incubated with APC-conjugated F(ab′)2-Goat anti-Mouse IgG (H+L) Secondary Antibody (eBioscience) and LIVE/DEAD™ Fixable Aqua Dead Cell Stain (Invitrogen) in PBS (30 min, 4 °C, dark). Alternatively, C1R cells were stained with eFluor780 and anti-MR1-PE (361106, 26.5; BioLegend). Cells were washed and fixed as in CD69 activation assays prior to acquisition on a BD LSRII or BD LSRFortessa flow cytometer using BD FACS Diva software. Data were analyzed using FlowJo v10 (BD).

MR1 Tetramer Staining of PBMCs. PBMCs were obtained from the Australian Red Cross Lifeblood (Agreement No. 22-08VIC-05) and isolated as described previously (18).

To generate tetramers, biotinylated MR1 monomers were incubated with streptavidin-PE (554061; BD Biosciences) at a 5:1 mass ratio by sequentially adding equal amounts of conjugated streptavidin every 10 min at room temperature in the dark. MR1 tetramers were diluted to a final monomer concentration of 0.25 mg/mL with TBS pH 8 and used at a 1:100 dilution.

PBMCs were stained with streptavidin-PE conjugated MR1 tetramers diluted in PBS + 2% FCS for 30 min at room temperature in the dark in preparation for enrichment as described previously (57). In brief, PBMCs were washed once and stained with anti-PE microbeads (130-097-054; Miltenyi Biotec) for 20 min at 4 °C. Microbead-labeled cells were washed twice and passed through an LS column (130-042-401; Miltenyi Biotec) under magnetic duress. MR1 tetramer bound PBMCs were eluted from the column and stained with anti-CD3-BUV395, anti-CD19-APC-Cy7 (302218, HIB19; BioLegend), anti-CD8α-BUV805 (612889, SK1; BD Horizon), anti-CD4-BUV496 (612936, SK3; BD Horizon), and eFluor780 diluted in PBS + 2% FCS for 30 min at 4 °C in the dark. Stained cells were washed twice and resuspended in 1% paraformaldehyde (PFA) in PBS before data acquisition on a BD LSR Fortessa.

MR1 Typing. DNA was isolated from cell lysates using BioRad Instagene matrix. The region of exon 2 encompassing codons for R9 and H17 was amplified to produce a 231 bp product using an upstream intronic forward primer (5′ ACATGTCTTCCTTCTTTGCCTC 3′), a downstream exonic reverse primer (5′ CCCTCAGCAGCTGAGTGTACC 3′) and QIAGEN Taq polymerase, following the manufacturer's instructions. Excess primers were removed using a QIAquick PCR purification kit. Sequencing reactions and electrophoresis were performed by Micromon genomics using the exonic reverse primer. Chromatograms were viewed with SnapGene Viewer (SnapGene software from Dotmatics; available at snapgene.com).

Fluorescence Polarization Assay. Various concentrations of the investigated compounds were incubated in competition with 10 nM TAMRA-conjugated JYM20 for binding 100 nM empty hMR1 protein in the Fluorescence Polarization assay buffer (25 mM HEPES, pH 7.5, 150 mM NaCl, 5 mM EDTA) (17). All compounds were dissolved in DMSO. The fluorescence polarization of TAMRA was measured after 24 h of incubation at 37 °C using a PHERAstar microplate reader (BMG LABTECH). The ligand-binding curves were simulated by nonlinear regression with Prism software (GraphPad Software Inc.) using a sigmoidal dose–response curve. The IC_{50} binding values were used as a measurement of the binding affinity and calculated as the ligand concentration required for 50% inhibition of JYM20 binding to MR1 molecules.

Expression and Preparation of Denatured Inclusion Bodies of MR1 and TCRs Proteins. Human A-F7 (TRAV1-2/TRBV6-1) MAITTCR proteins were refolded from inclusion bodies at 4 °C for an overnight period using the refolding buffer that contained 0.1 M Tris pH 8.5, 6 M urea, 2 mM EDTA, 0.4 M L-arginine, 0.5 mM oxidized glutathione, and 5 mM reduced glutathione as previously reported (28). The wild-type or C-terminal cysteine mutated MR1-β2 m was refolded at a 10× molar ratio of the investigated compound in the same refold buffer, as previously described (9). The refolded MR1-ligand and TCR proteins were purified using three sequential purification procedures: crude DEAE anion exchange, S200 15/60 size exclusion chromatography, and HiTrap-Q HP or MonoQ 10/100 GL anion exchange. After the protein's quality and purity were assessed using sodium dodecyl sulfate–polyacrylamide gel electrophoresis, it was concentrated and subjected to further measurements using a NanoDrop spectrophotometer.

Thermal Stability Assay. To investigate the thermostability of the WT and R9H mutant of MR1, a thermal shift assay was performed in a real-time detection system (RotorGene 3000). The fluorescent dye Sypro orange (Sigma) was used to monitor the protein unfolding upon heating. Human MR1 refolded with different ligands was purified by gel filtration directly before the experiment and eluted in buffer of 10 mM Tris-HCl (pH 8) and 150 mM NaCl. Then, the samples were heated from 25 to 95 °C with heating rate of 1 °C/min. The fluorescence intensity was measured (excitation at 530 nm and emission at 610 nm) and the unfolding process was followed. The half maximum melting point (Tm50) represents the temperature for which 50% of the protein is unfolded. The runs were conducted in triplicate, in three independent times.

Crystallization, Data Collection, Structure Determination, and Refinement. Purified A-F7 TCR was mixed with MR1-β2m-Ag in a 1:1 molar ratio and then held on ice for 2 h. The concentration of the mixture was 4 to 6 mg/mL. A-F7 TCR-MR1-Ag crystals were created at 20 °C using the hanging-drop vapor diffusion method, as previously reported (9). The precipitant reservoir solution consisted of 100 mM Bis–Tris Propane (BTP; pH 6.0 to 6.7), 10 to 20% PEG3350, and 200 mM sodium acetate. The ternary complex crystals were grown for 2 wk and harvested before being quickly soaked in reservoir solution containing 10 to 14% glycerol for cryoprotection and then flash-frozen in liquid nitrogen. At the Australian Synchrotron, X-ray diffraction datasets were collected at 100 K using the MX2 beamline. Diffraction data were processed using XDS (58) and programs from the CCP4 suite (59) and Phenix package (60).

The ternary structure of TCR-MR1-Ags complexes were solved using the previously solved A-F7 TCR and MR1 structures (PDB, 6PUC) (20) as a search model for molecular replacement in the PHASER program (61). The ligand restraints were built and generated using the Grade Webserver and Phenix tools. After building the models in COOT (62) and refining them iteratively with Phenix.refine (60), the models were validated with MolProbity (63). *SI Appendix*, Table S1 provides a summary of the panel of TCR-MR1-Ags final crystallographic data. The table of contacts was generated by the Contact program from the CCP4 suite (59). PyMOL Molecular Graphics System, Version 2.2 (Schrödinger, LLC, New York, NY) was used to create molecular graphics representations.

B6 Vitamer Quantification. A range of primary/healthy, immortalized, and cancerous cell lines were cultured for 24 to 72 h to allow for vitamer uptake and proliferation in cell-specific media: AML, K562, VMM1, PBMCs, and splenocytes were all cultured in RF10 media (as described for RF5 above but with 10% heat inactivated fetal calf serum). A549 and MM231 cell lines were cultured in DMEM-10 and 1,106 keratinocytes were cultured in Keratinocyte-serum free medium (Gibco 37000-015). PBMCs were obtained from the Australian Red Cross Lifeblood and isolated as described previously (18). Splenocytes were harvested from human spleen collected as part of the Australian Donation and Transplantation Biobank immediately after organ retrieval (Monash University Human ethics, Project ID: HREC27876).

Cell pellets were harvested by centrifugation of media-suspended cells (285 rcf for 5 min at RT), supernatant removal, and successive washes in 10 mL of ice-cold PBS (3 in total). Final cell pellets were snap-frozen in preweighed 2 mL lo-bind Eppendorf tubes and stored at −80 °C until further sample processing. On the day of analysis, cell pellets were weighed by mass difference with preweighed tubes, and combined with a 10 μL/mg of cell pellet ratio of 80% acetonitrile, 20% water, 0.1% formic acid. All pellets were homogenized using a 5 mm ball-bearing in a Qiagen TissueLyser LT for 4 min at 50 Hz. Homogenates were left to shake at RT for 10 min to reverse any vitamer Schiff-base bonds, before centrifugation at 15,000 rcf for 4 min to remove precipitated material. Supernatant was transferred to LC–MS vials for analysis using the same Thermo Q-Exactive Plus Orbitrap mass spectrometer and LC system outlined in earlier sections. Cell pellet lysates were quantified against standard curves of PL and PN prepared in 80% ACN.

Data, Materials, and Software Availability. The accession number for the atomic coordinates of A-F7 TCR-MR1*01 in complex with Pyridoxal and pyridoxal 5′-phosphate, along with associated structure factors, have been deposited at the protein databank (www.rcsb.org) with accession codes 9CGR and 9CGS, respectively (64, 65).

Note Added in Proof. We have recently become aware of a preprint that also reports Pyridoxal as a MR1 ligand using a different approach further substantiating our findings (see Schmidlin et al., Sneak Peek, MR1-Ligand Cross-Linking Identifies Vitamin B6 Metabolites as MAIT-TCR-Reactive Antigens. http://dx.doi.org/10.2139/ssrn.4979016).

ACKNOWLEDGMENTS. We acknowledge the Monash Biomedical Proteomics Facility, Monash University, for the provision of instrumentation, training, and technical support; Monash University FlowCore Facility for flow cytometry instrumentation, technical support, and sorting of cells; and the use of the services and facilities of Micromon Genomics at Monash University. We acknowledge the Melbourne Cytometry Platform (Peter Doherty Institute node) for provision of flow cytometry services and the Bio21 Institute Proteomics and Mass Spectrometry Facility. We thank the staff at the Monash Macromolecular Crystallization Facility. This research was undertaken in part using the MX2 beamline at the Australian Synchrotron, part of Australian Nuclear Science and Technology Organisation, and used the Australian Cancer Research Foundation detector. We acknowledge Austin Health and the Austin Health Researchers (Varun J. Sharma, Aly Fayed, Graham Starkey, Rohit D'Costa, Claire L. Gordon) for provision of splenocytes as part of the Australian Donation and Transplantation Biobank (ADTB). We gratefully acknowledge the generosity of the deceased organ donors and their families in providing valuable samples to the ADTB. This work was supported by a NIH (RO1 AI148407-01A1 to J.M., J.R., and D.P.F.); Australian Research Council (ARC) Discovery Grants DP220102401 to A.W.P. and J.R. and DP240102905 to J.M., M.N.T.S., and Z.C., an ARC Centre of Excellence Grant (CE200100012) to D.P.F, and a University of Melbourne Early Career Researcher Grant to M.N.T.S. W.A. is supported by an ARC Discovery Early Career Researcher Award (DE220101491). J.R., A.W.P., D.P.F., and J.M. are supported by Australian National Health and Medical Research Council Investigator Awards (2008981, 2016596, 2009551, and 2008616, respectively).

Author affiliations: [a]Department of Biochemistry and Molecular Biology and Immunity Program, Biomedicine Discovery Institute, Monash University, Clayton, VIC 3800, Australia; [b]Department of Microbiology and Immunology, The Peter Doherty Institute for Infection and Immunity, The University of Melbourne, Parkville, VIC 3052, Australia; [c]Centre for Chemistry and Drug Discovery and Australian Research Council Centre of Excellence for Innovations in Peptide and Protein Science, Institute for Molecular Bioscience, University of Queensland, Brisbane, QLD 4072, Australia; [d]Mass Spectrometry and Proteomics Facility, Bio21 Institute, The University of Melbourne, Parkville, VIC 3052, Australia; and [e]Institute of Infection and Immunity, Cardiff University, School of Medicine, Heath Park, Cardiff CF10 3AT, United Kingdom

1. I. Van Rhijn, D. I. Godfrey, J. Rossjohn, D. B. Moody, Lipid and small-molecule display by CD1 and MR1. *Nat. Rev. Immunol.* **15**, 643–654 (2015).
2. E. J. Adams, A. M. Luoma, The adaptable major histocompatibility complex (MHC) fold: Structure and function of nonclassical and MHC class I-like molecules. *Annu. Rev. Immunol.* **31**, 529–561 (2013).
3. M. Roerden, A. Nelde, J. S. Walz, Neoantigens in hematological malignancies-ultimate targets for immunotherapy? *Front. Immunol.* **10**, 3004 (2019).
4. P. T. Illing, S. H. Ramarathinam, A. W. Purcell, New insights and approaches for analyses of immunopeptidomes. *Curr. Opin. Immunol.* **77**, 102216 (2022).
5. T. P. Cao *et al.*, A structural perspective of how T cell receptors recognise the CD1 family of lipid antigen-presenting molecules. *J. Biol. Chem.* **300**, 107511 (2024), 10.1016/j.jbc.2024.107511.
6. S. Huang *et al.*, CD1 lipidomes reveal lipid-binding motifs and size-based antigen-display mechanisms. *Cell* **186**, 4583–4596.e4513 (2023).
7. L. J. Howson *et al.*, Absence of mucosal-associated invariant T cells in a person with a homozygous point mutation in MR1. *Sci. Immunol.* **5**, eabc9492 (2020).
8. E. Rozemuller *et al.*, MR1 encompasses at least six allele groups with coding region alterations. *Hla* **98**, 509–516 (2021).
9. A. J. Corbett *et al.*, T-cell activation by transitory neo-antigens derived from distinct microbial pathways. *Nature* **509**, 361–365 (2014).
10. L. Kjer-Nielsen *et al.*, MR1 presents microbial vitamin B metabolites to MAIT cells. *Nature* **491**, 717–723 (2012).
11. J. Y. Mak *et al.*, Stabilizing short-lived Schiff base derivatives of 5-aminouracils that activate mucosal-associated invariant T cells. *Nat. Commun.* **8**, 14599 (2017).
12. J. Y. W. Mak, L. Liu, D. P. Fairlie, Chemical modulators of mucosal associated invariant T cells. *Acc. Chem. Res.* **54**, 3462–3475 (2021).
13. E. Ito *et al.*, Sulfated bile acid is a host-derived ligand for MAIT cells. *Sci. Immunol.* **9**, eade6924 (2024).
14. A. Vacchini *et al.*, Nucleobase adducts bind MR1 and stimulate MR1-restricted T cells. *Sci. Immunol.* **9**, eadn0126 (2024).
15. M. Salio *et al.*, Ligand-dependent downregulation of MR1 cell surface expression. *Proc. Natl. Acad. Sci. U.S.A.* **117**, 10465–10475 (2020).
16. A. N. Keller *et al.*, Drugs and drug-like molecules can modulate the function of mucosal-associated invariant T cells. *Nat. Immunol.* **18**, 402–411 (2017).
17. C. J. H. Wang *et al.*, Quantitative affinity measurement of small molecule ligand binding to major histocompatibility complex class-I-related protein 1 MR1. *J. Biol. Chem.* **298**, 102714 (2022).
18. R. Reantragoon *et al.*, Antigen-loaded MR1 tetramers define T cell receptor heterogeneity in mucosal-associated invariant T cells. *J. Exp. Med.* **210**, 2305–2320 (2013).
19. N. A. Gherardin *et al.*, Diversity of T cells restricted by the MHC class I-related molecule MR1 facilitates differential antigen recognition. *Immunity* **44**, 32–45 (2016).
20. W. Awad *et al.*, The molecular basis underpinning the potency and specificity of MAIT cell antigens. *Nat. Immunol.* **21**, 400–411 (2020).
21. E. W. Meermeier *et al.*, Human TRAV1-2-negative MR1-restricted T cells detect *S. pyogenes* and alternatives to MAIT riboflavin-based antigens. *Nat. Commun.* **7**, 12506 (2016).
22. M. Lepore *et al.*, Functionally diverse human T cells recognize non-microbial antigens presented by MR1. *eLife* **6**, e24476 (2017).
23. M. D. Crowther *et al.*, Genome-wide CRISPR–Cas9 screening reveals ubiquitous T cell cancer targeting via the monomorphic MHC class I-related protein MR1. *Nat. Immunol.* **21**, 178–185 (2020).
24. T. V. Cornforth *et al.*, Conserved allomorphs of MR1 drive specificity of MR1-restricted TCRs. *Front. Oncol.* **14**, 1419528 (2024).
25. F. Tilloy *et al.*, An invariant T cell receptor alpha chain defines a novel TAP-independent major histocompatibility complex class Ib-restricted alpha/beta T cell subpopulation in mammals. *J. Exp. Med.* **189**, 1907–1921 (1999).
26. L. Kjer-Nielsen *et al.*, An overview on the identification of MAIT cell antigens. *Immunol. Cell Biol.* **96**, 573–587 (2018).
27. H. E. McWilliam *et al.*, The intracellular pathway for the presentation of vitamin B-related antigens by the antigen-presenting molecule MR1. *Nat. Immunol.* **17**, 531–537 (2016).
28. S. B. Eckle *et al.*, A molecular basis underpinning the T cell receptor heterogeneity of mucosal-associated invariant T cells. *J. Exp. Med.* **211**, 1585–1600 (2014).
29. H. Tsugawa *et al.*, MS-DIAL: Data-independent MS/MS deconvolution for comprehensive metabolome analysis. *Nat. Methods* **12**, 523–526 (2015).
30. K. Dührkop *et al.*, SIRIUS 4: A rapid tool for turning tandem mass spectra into metabolite structure information. *Nat. Methods* **16**, 299–302 (2019).
31. Z. Zhao *et al.*, Francisella tularensis induces Th1 like MAIT cells conferring protection against systemic and local infection. *Nat. Commun.* **12**, 4355 (2021).
32. M. N. T. Souter *et al.*, CD8 coreceptor engagement of MR1 enhances antigen responsiveness by human MAIT and other MR1-reactive T cells. *J. Exp. Med.* **219**, e20210828 (2022).
33. A. Chancellor *et al.*, Promiscuous recognition of MR1 drives self-reactive mucosal-associated invariant T cell responses. *J. Exp. Med.* **220**, e20221939 (2023).
34. J. Y. W. Mak *et al.*, Potent immunomodulators developed from an unstable bacterial metabolite of vitamin B2 biosynthesis. *Angew. Chem. Int. Ed. Engl.* **63**, e202400632 (2024), 10.1002/anie.202400632.
35. R. Percudani, A. Peracchi, A genomic overview of pyridoxal-phosphate-dependent enzymes. *EMBO Rep.* **4**, 850–854 (2003).
36. P. Wang *et al.*, Associations of serum vitamin B6 status with the risks of cardiovascular, cancer, and all-cause mortality in the elderly. *Front. Immunol.* **15**, 1354958 (2024).
37. E. Pilesi *et al.*, Vitamin B6 deficiency cooperates with oncogenic Ras to induce malignant tumors in *Drosophila*. *Cell Death Dis.* **15**, 388 (2024).
38. X. Li *et al.*, Targeting PNPO to suppress tumor growth via inhibiting autophagic flux and to reverse paclitaxel resistance in ovarian cancer. *Apoptosis* **29**, 1546–1563 (2024), 10.1007/s10495-024-01956-3.
39. C. N. Franco *et al.*, Vitamin B(6) is governed by the local compartmentalization of metabolic enzymes during growth. *Sci. Adv.* **9**, eadi2232 (2023).
40. L. Xu *et al.*, Association of serum pyridoxal-5′-phosphate, pyridoxal, and PAr with colorectal cancer risk: A large-scale case–control study. *Nutrients* **14**, 2389 (2022).
41. P. Schorgg *et al.*, Increased vitamin B6 turnover is associated with greater mortality risk in the general US population: A prospective biomarker study. *Clin. Nutr.* **41**, 1343–1356 (2022).
42. A. Joseph, J. Pan, J. Michels, G. Kroemer, M. Castedo, Pyridoxal kinase and poly(ADP-ribose) affect the immune microenvironment of locally advanced cancers. *Oncoimmunology* **10**, 1950954 (2021).
43. D. Bargiela *et al.*, Vitamin B6 metabolism determines T cell anti-tumor responses. *Front. Immunol.* **13**, 837669 (2022).
44. B. Qian, S. Shen, J. Zhang, P. Jing, Effects of vitamin B6 deficiency on the composition and functional potential of T cell populations. *J. Immunol. Res.* **2017**, 2197975 (2017).

45. G. P. Tryfiates *et al.*, Vitamin B6 and cancer: Synthesis and occurrence of adenosine-N6-diethylthioether-N-pyridoximine-5′-phosphate, a circulating human tumor marker. *Cancer Res.* **56**, 3670–3677 (1996).
46. G. P. Tryfiates, R. E. Bishop, Vitamin B6 and cancer: Adenosine-N6-diethylthioether N1-pyridoximine 5′-PO_4, a circulating human tumor marker. *Anticancer Res.* **15**, 379–383 (1995).
47. C. C. Chen *et al.*, Vitamin B6 addiction in acute myeloid leukemia. *Cancer Cell* **37**, 71–84.e77 (2020).
48. L. Galluzzi *et al.*, Effects of vitamin B6 metabolism on oncogenesis, tumor progression and therapeutic responses. *Oncogene* **32**, 4995–5004 (2013).
49. J. Y. W. Mak, Determination of sample concentrations by PULCON NMR spectroscopy. *Aust. J. Chem.* **75**, 160–164 (2022).
50. A. W. Purcell, S. H. Ramarathinam, N. Ternette, Mass spectrometry–based identification of MHC-bound peptides for immunopeptidomics. *Nat. Protoc.* **14**, 1687–1707 (2019).
51. R. Reantragoon *et al.*, Structural insight into MR1-mediated recognition of the mucosal associated invariant T cell receptor. *J. Exp. Med.* **209**, 761–774 (2012).
52. T. H. O. Nguyen *et al.*, Cross-reactive anti-viral T cells increase prior to an episode of viral reactivation post human lung transplantation. *PLoS ONE* **8**, e56042 (2013).
53. F. A. Ran *et al.*, Genome engineering using the CRISPR-Cas9 system. *Nat. Protoc.* **8**, 2281–2308 (2013).
54. K. Labun *et al.*, CHOPCHOP v3: Expanding the CRISPR web toolbox beyond genome editing. *Nucleic Acids Res.* **47**, W171–W174 (2019).
55. M. Goncharov *et al.*, VDJdb in the pandemic era: A compendium of T cell receptors specific for SARS-CoV-2. *Nat. Methods* **19**, 1017–1019 (2022).
56. E. J. Grant *et al.*, Lack of heterologous cross-reactivity toward HLA-A*02:01 restricted viral epitopes is underpinned by distinct αβT cell receptor signatures. *J. Biol. Chem.* **291**, 24335–24351 (2016).
57. M. N. T. Souter *et al.*, Characterization of human mucosal-associated invariant T (MAIT) cells. *Curr. Protoc. Immunol.* **127**, e90 (2019).
58. W. Kabsch, Integration, scaling, space-group assignment and post-refinement. *Acta Crystallogr., Sect. D, Biol. Crystallogr.* **66**, 133–144 (2010).
59. M. D. Winn *et al.*, Overview of the CCP4 suite and current developments. *Acta Crystallogr., Sect. D, Biol. Crystallogr.* **67**, 235–242 (2011).
60. P. D. Adams *et al.*, PHENIX: A comprehensive Python-based system for macromolecular structure solution. *Acta Crystallogr., Sect. D, Biol. Crystallogr.* **66**, 213–221 (2010).
61. A. J. McCoy, Solving structures of protein complexes by molecular replacement with Phaser. *Acta Crystallogr., Sect. D, Biol. Crystallogr.* **63**, 32–41 (2007).
62. P. Emsley, K. Cowtan, Coot: Model-building tools for molecular graphics. *Acta Crystallogr., Sect. D, Biol. Crystallogr.* **60**, 2126–2132 (2004).
63. V. B. Chen *et al.*, MolProbity: All-atom structure validation for macromolecular crystallography. *Acta Crystallogr., Sect. D, Biol. Crystallogr.* **66**, 12–21 (2010).
64. W. Awad, J. Rossjohn, TCR-MR1-PL. RCSB PDB. https://doi.org/10.2210/pdb9cgr/pdb. Deposited 30 August 2024.
65. W. Awad, J. Rossjohn, TCR-MR1-PLP. RCSB PDB. https://doi.org/10.2210/pdb9cgs/pdb. Deposited 30 August 2024.